Published in IET Power Electronics
Received on 24th March 2012
Revised on 26th June 2012
doi: 10.1049/iet-pel.2012.0135

ISSN 1755-4535

Improving dynamic performance of wind energy conversion systems using fuzzy-based hysteresis current-controlled superconducting magnetic energy storage

A.M. Shiddiq Yunus[1] *A. Abu-Siada*[2] *M.A.S. Masoum*[2]

[1]*Energy Conversion Study Program, Mechanical Engineering Department, Polytechnic State of Ujung Pandang, South-Sulawesi 90245, Indonesia*
[2]*Department of Electrical and Computer Engineering, Curtin University, Perth, WA 6845, Australia*
E-mail: a.abusiada@curtin.edu.au

Abstract: Application of distributed wind energy conversion systems (WECS) in modern power systems and smart grids has significantly increased during the last decade. In particular, wind turbines equipped with doubly fed induction generator (DFIG) have dominated the market since 2004 as they represented about 55% of the worldwide total wind capacity during this year. This study investigates the application of superconducting magnetic energy storage (SMES) units to improve the dynamic performance of DFIG-based WECS during small and large disturbances in the grid side. A new control approach for the SMES unit using hysteresis current regulator and fuzzy logic is introduced. Detailed simulation results show that the proposed SMES controller is very effective in improving the dynamic performance of the WECS and is able to maintain its parameters within the safety margins of various grid codes during disturbance events considered in this study.

1 Introduction

Wind power installation is significantly increasing globally. In 2010, the growth rate in wind power generation worldwide was 23.6% although the global wind power capacity is expected to reach 600 and 150 GW by the years 2015 and 2020, respectively [1]. The annual renewable energy generation in Australia is about 5100 GWh and the government has set a 20% renewable energy generation target by the year 2020 [2]. Doubly fed induction generator (DFIG) is one of the most popular variable speed wind turbine generators [3]. Compared with fixed speed wind turbines, DFIG has the advantage of capturing maximum power, improved power quality, reduced mechanical stress imposed on the turbine during wind fluctuation and decoupled active and reactive power control [4].

In the earlier stages of integrating wind energy conversion systems (WECS) into the electricity grids, wind turbines were disconnected from the grid during faults at the grid side to avoid any possible damages to them. Recently, the existing wind turbine generators, however, have been designed/managed to comply with the recent requirements of the new grid codes [5] to ensure the continuity of supplying power to the grid during transient and abnormal operating conditions. There are two strategies that can be adopted to improve the performance or the fault ride-through (FRT) capability of the DFIG. The first approach is to develop new control techniques to fulfil the requirements of the transmission system operators (TSOs) as presented in most of the literatures [6–9]; however, this strategy is only effective for new installation of WECS. The second approach is to incorporate flexible AC transmission system (FACTS) devices to improve the dynamic performance of the DFIG during disturbance events and hence comply with the TSO requirements [10]. The latter option is a more cost-effective choice for the existing WECS.

There are some publications in the literature investigating the application of the superconducting magnetic energy storage (SMES) unit to smooth the output power of fixed speed-based WECS during wind speed fluctuation to avoid system instability [11–18]. A few studies considered the application of the SMES unit to improve the dynamic performance of variable speed-based WECS such as in [19, 20]. However, the SMES controller proposed in [19] is applicable only for new and low capacity scale of WECS constructions. Moreover, adopting this approach is not a cost-effective choice since it calls for replacing the existing WECS by new ones to accommodate the proposed approach. In [20], the 1000 MW scale of DFIG is connected to the high voltage direct current (HVDC) line whereas the SMES is connected in the middle of the DC line, which is an impractical location for the SMES unit. Also, the SMES configuration is not presented in this study and the simulation results show the limitation of the proposed controller in suppressing the impact of DC-line faults.

Owing to this limitation an extra static synchronous compensator (STATCOM) is proposed to be connected to the system along with the SMES unit.

This paper introduces a new application along with a new control approach for the SMES unit, to improve the dynamic performance of the WECS during small and large disturbances in the grid side. The advantages of the proposed controller are highlighted in Section 3.

2 DFIG equivalent circuit and system under study

A typical configuration of DFIG under study is shown in Fig. 1*a*. The stator winding is directly connected to a coupling transformer low-voltage side, whereas the rotor winding is connected to bidirectional back-to-back IGBT voltage source converters. The converter helps in decoupling the mechanical and electrical frequencies and facilitates variable speed operation. As the DFIG is equipped with a partial scale converter, the turbine cannot operate in full range from zero to rated speed; however, the speed range is proven to be quite sufficient [3].

Simplifying the model of the DFIG without losing model accuracy is possible with the 'Γ-form' equivalent circuit of Fig. 1*b* [21]. As the detailed analysis of DFIG in 'Γ-form' is available and discussed in [22–24], a brief presentation of the key equations is provided here.

The stator and rotor voltage vectors in the arbitrary reference frame are given as

$$\boldsymbol{V}_{\mathrm{s}} = R_{\mathrm{s}} I_{\mathrm{s}} \frac{\mathrm{d}\boldsymbol{\lambda}_{\mathrm{s}}}{\mathrm{d}t}\ \mathrm{j}\omega\boldsymbol{\lambda}_{\mathrm{s}} \tag{1}$$

$$\boldsymbol{V}_{\mathrm{r}} = R_{\mathrm{r}} I_{\mathrm{r}} \frac{\mathrm{d}\boldsymbol{\lambda}_{\mathrm{r}}}{\mathrm{d}t}\ \mathrm{j}(\omega - \omega_{\mathrm{r}})\boldsymbol{\lambda}_{\mathrm{r}} \tag{2}$$

where ω is the angular speed and subscripts 's' and 'r' indicate stator and rotor parameters/quantities, respectively, as shown in the Appendix.

From Fig. 1*b*, the flux space vectors of stator and rotor can be expressed as

$$\boldsymbol{\lambda}_{\mathrm{s}} = L_{\mathrm{m}} I_{\mathrm{m}} \tag{3}$$

$$\boldsymbol{\lambda}_{\mathrm{r}} = L_{\sigma} I_{\mathrm{r}} + L_{\mathrm{m}} I_{\mathrm{m}} \tag{4}$$

where L_{m} is the magnetising inductance and L_{σ} is the leakage inductance. Since $I_{\mathrm{m}} = I_{\mathrm{s}} + I_{\mathrm{r}}$ the stator current can be calculated as

$$I_{\mathrm{s}} = \frac{\boldsymbol{\lambda}_{\mathrm{s}}}{L_{\mathrm{m}}} - I_{\mathrm{r}} \tag{5}$$

A speed variation of $\pm 30\%$ around synchronous speed can be obtained by the use of a relatively small power converter rated at 30% of the DFIG nominal power [25]. The electrical power is delivered to the grid through the rotor and the stator if the generator is running in a super-synchronous mode. If the generator is running in a sub-synchronous mode, electrical power is delivered into the rotor from the grid.

Both single-stage (DFIG-1G) and three-stage (DFIG-3G) gear box type of DFIG have lower total cost when compared with similar types of the permanent magnet synchronous generator (PMSG) as illustrated in Figs. 2*a* and *b* [26]. The cost study in [26] shows that the highest cost portion in all WECS types is allocated for the gear box, whereas the higher cost of PMSG is owing to its full size converter price, which is almost double of the one-third converter size used by the DFIG. The fixed speed-based WECS is generally more cost-effective compared with DFIG and PMSG types as it does not require any power electronic interface. However, the superior technical benefits of variable speed-based WECS have resulted in a significant decrease in fixed speed-based WECS installation since 1995 [4].

Fig. 3 shows the system under study, which consists of six-1.5 MW DFIG connected to the grid through a 45 km

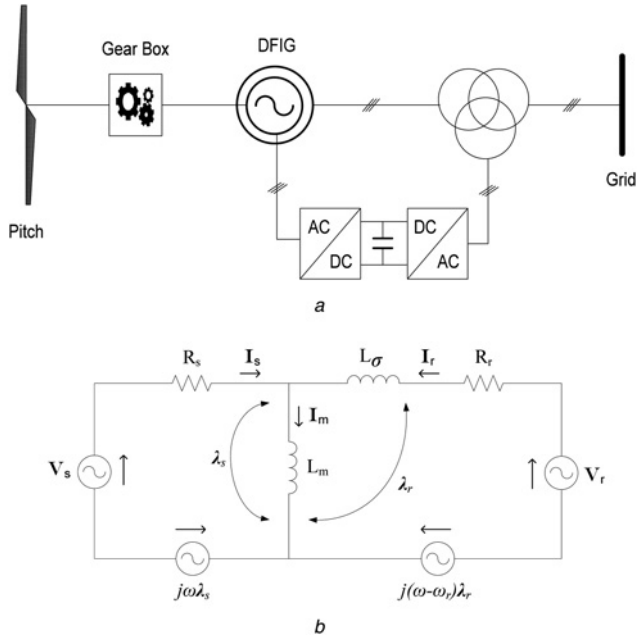

Fig. 1 *DFIG equivalent circuit and system under study*

a Typical configuration of DFIG
b Equivalent circuit of DFIG in Γ-form

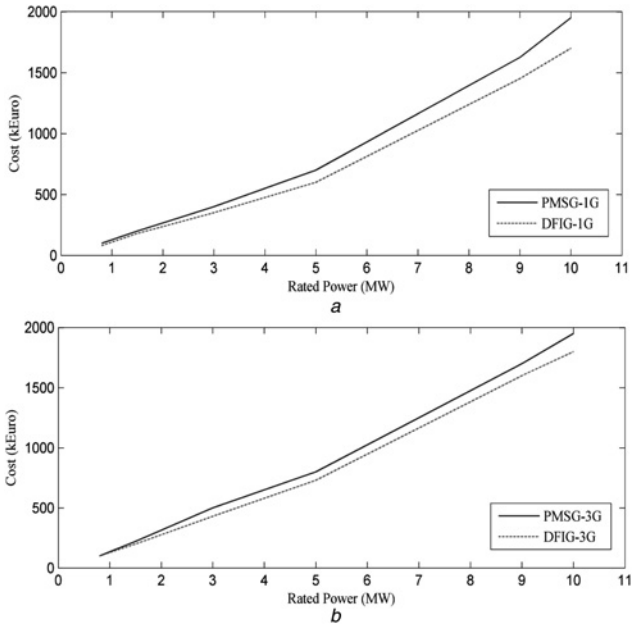

Fig. 2 *Both DFIG-1G and DFIG-3G gear box type of DFIG*

a Cost comparison of DFIG-1G against PMSG-1G
b Cost comparison of DFIG-3G against PMSG-3G [26]

doi: 10.1049/iet-pel.2012.0135

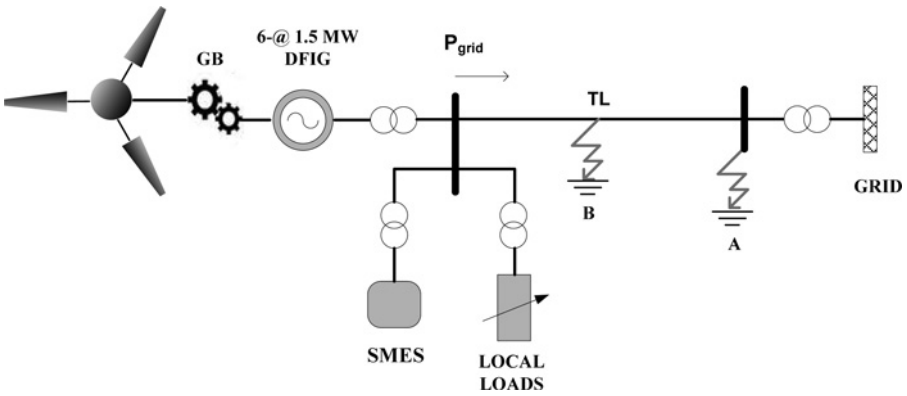

Fig. 3 *System under study*

transmission line. A local AC load is connected to the DFIG bus to allow dynamic stability studies. During normal operation, the local load is fed by the DFIG and the remaining generated power is transferred to the grid, which is represented by an ideal three-phase voltage source of constant frequency through the transmission line. For an average wind speed of 15 m/s, which is used in this study, the wind turbine is assumed to operate at unitypower factor and generates 1.0 pu active power with a shaft speed of 1.2 pu. The SMES unit is connected to the DFIG bus and is assumed to be fully charged at its maximum capacity of 1.0 MJ.

3 SMES configuration and control scheme

A superconducting coil stores energy within a magnetic field created by the flow of direct current in a coil, which should be maintained within the superconductivity state through immersion in liquid helium at 4.2 K in a vacuum – insulated cryostat. A power electronic converter interfaces the SMES and the grid to control the energy exchange between them. With the rapid development of materials that exhibit superconductivity closer to room temperatures, the SMES technology is expected to become economically viable in the next few years [27]. The overall efficiency of the SMES, which is in a typical range of 90–98% depends on the coil material and the configuration used [12, 28, 29]. The high efficiency of the SMES unit is attributed to its lower power loss as the electric current in the coil encounters almost no resistance and there are no moving parts included. The configuration of the SMES unit used in this paper is shown in Fig. 4*a*.

Generally, there are two major configurations of SMES; current source converter (CSC) and voltage source converter (VSC). Traditionally, CSC is connected through a 12-pulse converter configuration to eliminate the AC side fifth and seventh harmonic currents and the DC side sixth harmonic voltage, thus resulting in a significant saving in harmonic filters [30]. However, because this configuration uses two six-pulse CSCs that are connected in parallel, its cost is relatively high. On the other hand, VSC is connected with a DC–DC chopper through a DC link to facilitate energy exchange between the SMES coil and the AC grid. Hassan *et al.* [31] estimate the total cost of switching devices of the CSC to be 173% of the switching devices

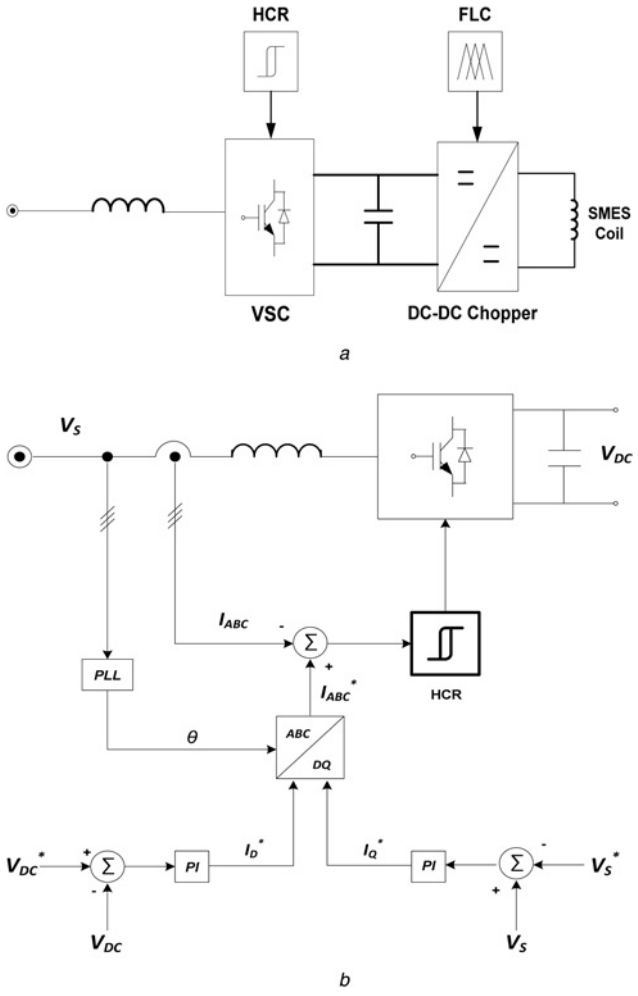

Fig. 4 *Configuration of SMES and VSC control schemes*
a SMES configuration
b VSC control scheme

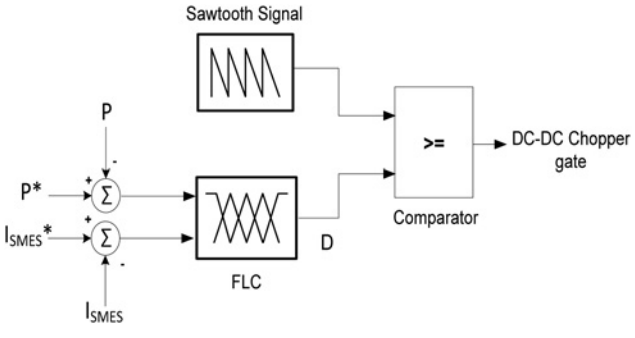

Fig. 5 *Fuzzy logic control scheme*

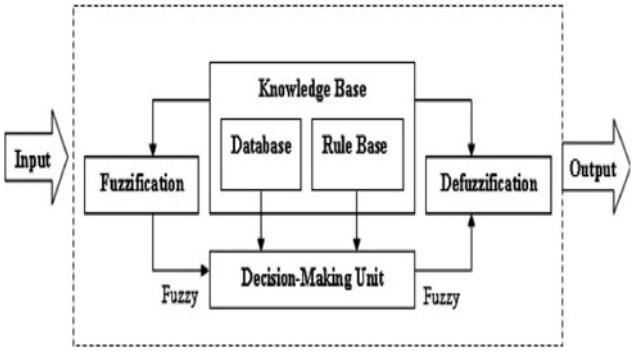

Fig. 6 *Fuzzy inference flowchart*

Table 1 Rules of duty cycle

Duty cycle (D)	SMES coil action
$D = 0.5$	standby condition
$0 \leq D < 0.5$	discharging condition
$0.5 < D \leq 1$	charging condition

and power diodes required for equivalent capacity of the VSC and the chopper. Moreover, a VSC has a better self-commutating capability and it injects lower harmonic currents into the AC grid than a comparable CSC. The use of insulated-gate bipolar transistor (IGBT) in this

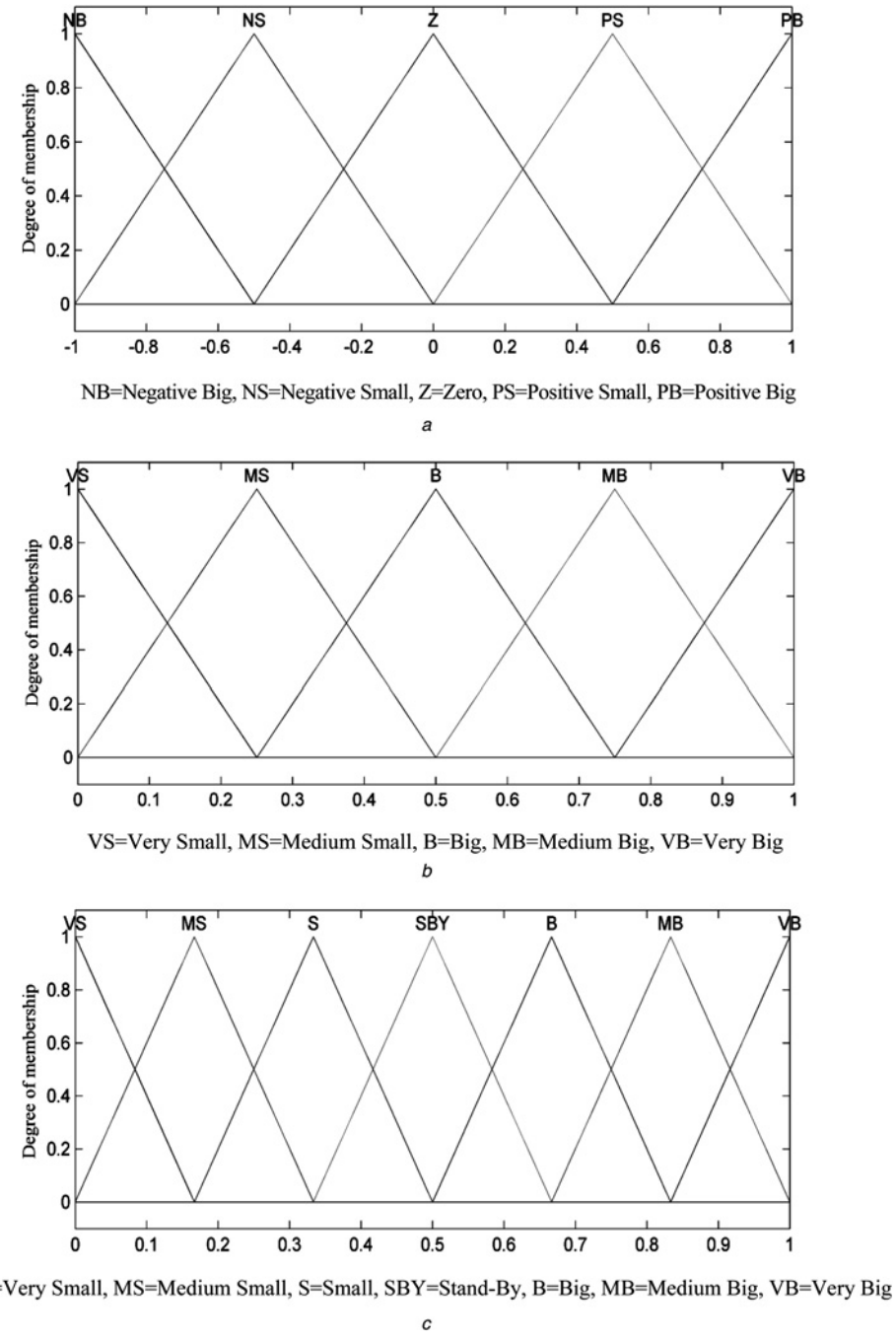

Fig. 7 *Corresponding MFs for each input and output variable*

a Input variable MF–ΔP
b Input variable MF–ΔI_{SMES}
c Output variable MF–duty cycle (D)

doi: 10.1049/iet-pel.2012.0135

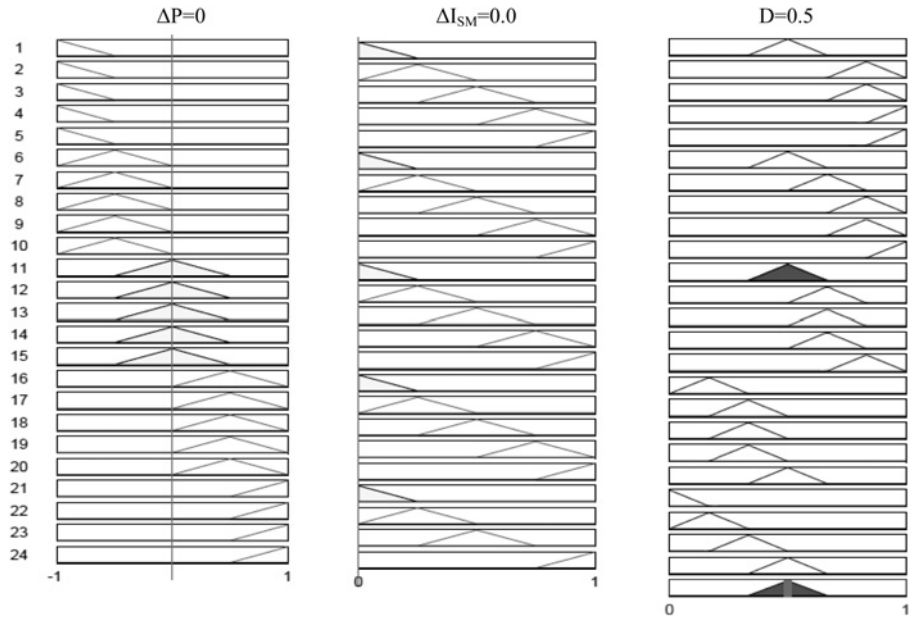

Fig. 8 *Fuzzy logic rules*

configuration is more beneficial than gate turn-off thyristor (GTO) since the switching frequency of an IGBT lies on the range of 2–20 kHz, whereas in the case of GTO, the switching frequency does not exceed 1 kHz [32]. In this paper, a hysteresis current regulator along with a fuzzy logic controller (FLC) (shown in Fig. 4*b*) are proposed to control the active and reactive power exchange between the SMES unit and the grid as will be explained in the following subsections.

Although the control system of the DC–DC chopper is presented in [33], the control approach for the VSC as a part of the SMES configuration is not discussed. In contrast with [33], the DC–DC chopper control system is not presented in [11]. The configuration of the SMES in [19] is technically new but its application is limited for low WECS capacity and since the SMES coil is proposed to be connected to the individual DFIG's converters, this topology will be only appropriate for new WECS installations. Application of the SMES unit to stabilise the micro-grid system is presented in [34]. The control scheme presented in this work is very complex because it is operating at three different levels of controls, which require a robust computational system; this will lead to a high implementation and maintenance cost.

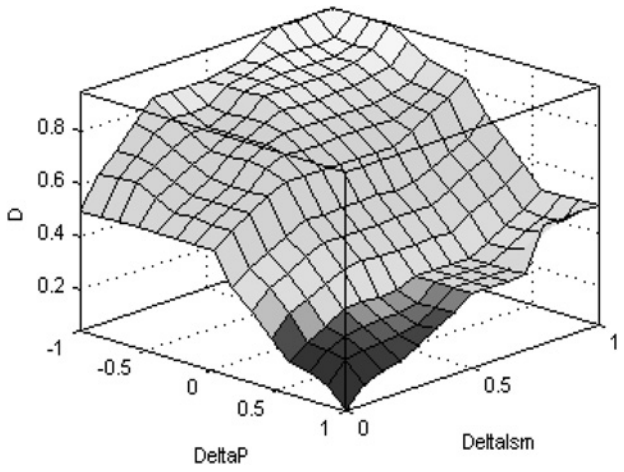

Fig. 9 *Surface-graph relationship between input and output of fuzzy rules*

The proposed control algorithm in this paper is much simpler and closer to realistic applications compared with the controller implemented in [13], where four proportional-integral (PI) controllers were used. Moreover, the proposed controller in [13] only uses the DFIG generated active power (P_g) as a feedback signal to the DC–DC chopper while it ignores the energy capacity of the SMES unit. The proposed control scheme in this paper comprises only two PI controllers and considers the SMES stored energy capacity along with the DFIG generated power as control parameters to determine the direction and level of power exchange between the SMES coil and the AC system. This control system is efficient, simple and is easy to implement.

3.1 Hysteresis current regulator

To control the power exchange between the SMES unit and the AC system, the hysteresis current regulator is preferred based on its advantages, which include simple implementation, fast dynamic response, maximum current limit and its insensitivity to load parameter variations [35]. The solid state switching component of the VSC consists of six-IGBT switches to support the optimal application of the SMES unit since it simplifies converter design and enables a considerable higher switching frequency compared with a bipolar junction transistor [36]. The charging and discharging process of SMES energy is determined by an FLC of a DC–DC chopper, which is connected to the VSC through a DC link. The DC-link capacitor is used to achieve a constant DC voltage that is maintained by the VSC controller. The DFIG generated active power and the current pass through the superconductor coil and are used as inputs to the FLC. The hysteresis current regulator is used to control the power flow exchange between the grid and the SMES unit, which is performed by comparing the three-phase line currents with the reference current that are indicated by I_d^* and I_q^*, respectively. The values of I_d^* and I_q^* are generated through the conventional PI

controllers both from the error values of V_{DC} and V_s as shown in Fig. 4*b*.

3.2 Fuzzy logic controller

To determine the value of the duty cycle of the chopper, the real power and the SMES coil current are used as inputs to the FLC. The duty cycle is compared with a 1000 Hz sawtooth signal to provide a proper gate signal to the DC–DC chopper as shown in Fig. 5. The controller is developed in accordance with the fuzzy-inference flowchart shown in Fig. 6, which is a process of formulating the mapping from a given input to a designated output.

The rules for duty cycle (D) and the corresponding SMES action are shown in Table 1. It is assumed that the SMES unit is fully charged when connected to the system. When D is equal to 0.5, the SMES unit is in idle (standby) condition and there is no power exchange between the SMES unit and the grid. When there is any voltage drop because of any external fault, the controller generates a duty cycle in the range of 0–0.5 according to the value of the two input signals and energy will be transferred from the SMES coil to the grid. The charging action (corresponding to a duty cycle higher than 0.5) will take place when the SMES coil capacity is dropped and energy will be transferred from the grid to the charged SMES coil.

The model is built using the graphical user interface tool provided by MATLAB. Each input is fuzzified into five sets of trimf type of membership function (MF). The triangular MF is a function of a vector $\boldsymbol{x}$ and depends on three scalar parameters a, b and c as given by

$$f(\boldsymbol{x}, a, b, c) = \max\left(\min\left(\frac{\boldsymbol{x}-a}{b-a}, \frac{c-\boldsymbol{x}}{c-b}\right), 0\right) \quad (6)$$

a and c parameters locate the 'feet' of the triangle, whereas the b parameter locates the peak. The corresponding MFs for each input variable are shown in Figs. 7*a* and *b*.

The result of fuzzification from each input is then applied with a fuzzy operator in the antecedent and related to the consequence. The MFs for the output variables (duty cycle) are considered on the scale 0–1 as shown in Fig. 7*c*.

Centre-of-gravity, which is widely used in fuzzy models, is used for defuzzification of variables where the desired output z_0 is calculated as [37]

$$z_0 = \frac{\int z\mu_c(z)\,dz}{\int \mu_c(z)\,dz} \quad (7)$$

where $\mu_c(z)$ is the MF of the output.

A set of fuzzy rules that relates the input variables to the output variables according to Table 1 is developed according to system requirements as shown in Fig. 8, which shows that when there is no change to the DFIG active power and the SMES coil current, the duty cycle is maintained at 0.5 and no power exchange will take place between the SMES and the AC grid. Any change in these parameters owing to any fault condition, will change the duty cycle accordingly. The duty cycle for any set of input data (P and I_{SMES}) can also be evaluated using the surface graph shown in Fig. 9.

4 Simulation results and discussion

To examine the robustness of the proposed controller in enhancing the DFIG-based WECS dynamic performance, three fault scenarios are assumed and simulated as elaborated below.

4.1 Small disturbance

The load frequency control issue occurs in power systems as a result of sudden and small load perturbation, which creates an instantaneous mismatch between real generated power and load demand. This problem can be controlled by the

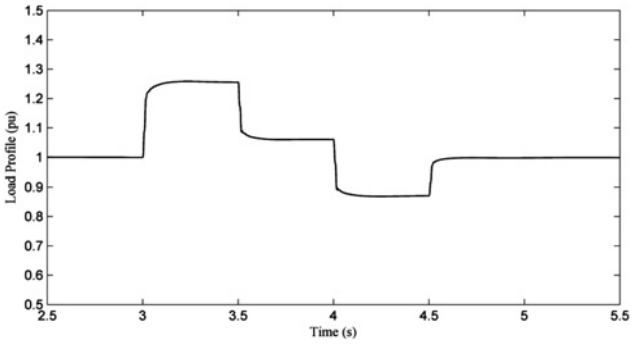

Fig. 10 *Load profile under study*

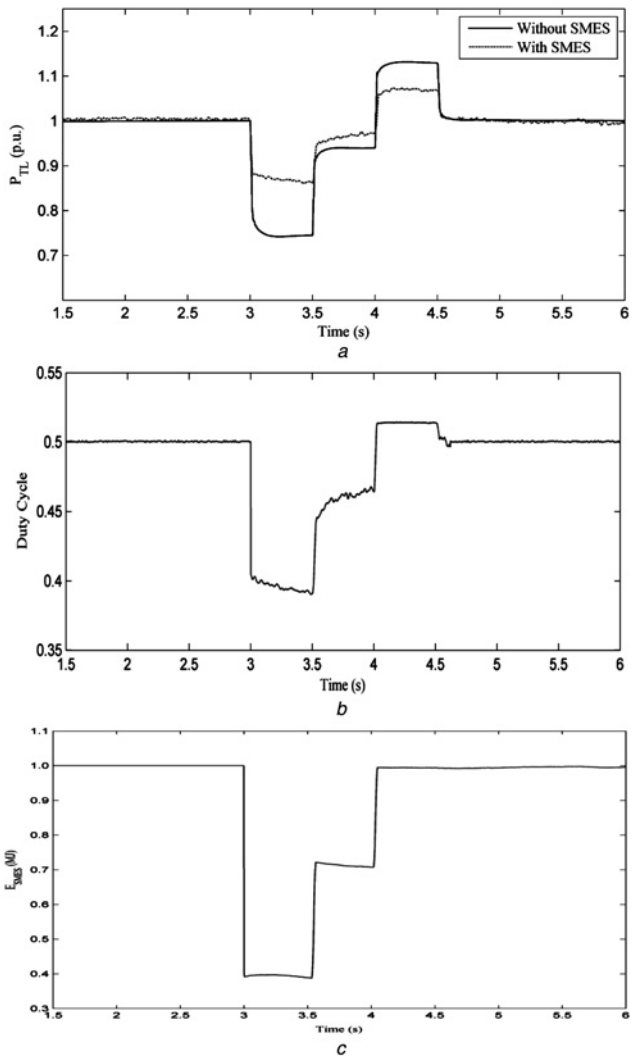

Fig. 11 *During dynamic events of SMES*

a Power transfer to the grid
b Duty cycle response during dynamic event
c Stored energy of SMES during dynamic event

doi: 10.1049/iet-pel.2012.0135

governor action in conventional thermal power plants. The load frequency control problem is attributed to the fact that the inertia of the rotating parts is the only storage capacity in a conventional power system where the additional power demand can be met through the kinetic energy of the generator rotor. This will limit the degree to which frequency deviation can be minimised by appropriate governor control. The problem is more serious in case of DFIG-based WECS in which the inertia is much lower than their power rating. Solving this problem by attaching a flywheel to the rotor shaft to increase its inertia will significantly increase the torsional stress on the shaft during a dynamic oscillation. Since the wind turbine generated power depends on wind speed, which cannot be controlled, the wind turbine can only be down-regulated to match the power demand when the load is decreased by applying additional controllers [32]. However, when the loads are increased above the rated power output of the generators, in particular when the wind speed is low, a power imbalance will take place causing a load frequency control problem. Adding an SMES unit, which has a very fast time response to the load bus can improve the system overall performance during such conditions.

Fig. 10 shows the load profile assumed in the simulation studies. It is assumed that the nominal load power is constant under normal operating conditions and is fed through the power generated from the wind turbine. The load is assumed to experience a ± 0.2 pu fluctuation for a duration of 0.5 s at $t = 3$ and $t = 4$ s, respectively.

Fig. 11*a* shows the power transferred to the grid through the transmission line. When the load power demand increases at $t = 3$ s, the power transfer through the transmission line decreases by 30% and it increases by only 10% because of the thermal limit of the transmission line when the load is decreased at $t = 4$ s. By connecting the SMES unit to the DFIG bus, the transmission line power transfer profile is substantially improved under load fluctuation as it will limit the upper and lower limits to only 10 and 5%, respectively. The duty cycle D of the DC–DC chopper is shown in Fig. 11*b* where at normal operating condition, the value of D is maintained by the FLC at a level of 0.5 and the SMES coil current is held constant at its rated value, consequently, there is no energy exchange between the SMES unit and the grid as can be shown from the coil stored energy in Fig. 11*c*. When the load increases suddenly at $t = 3$ s, the controller acts to decrease the value

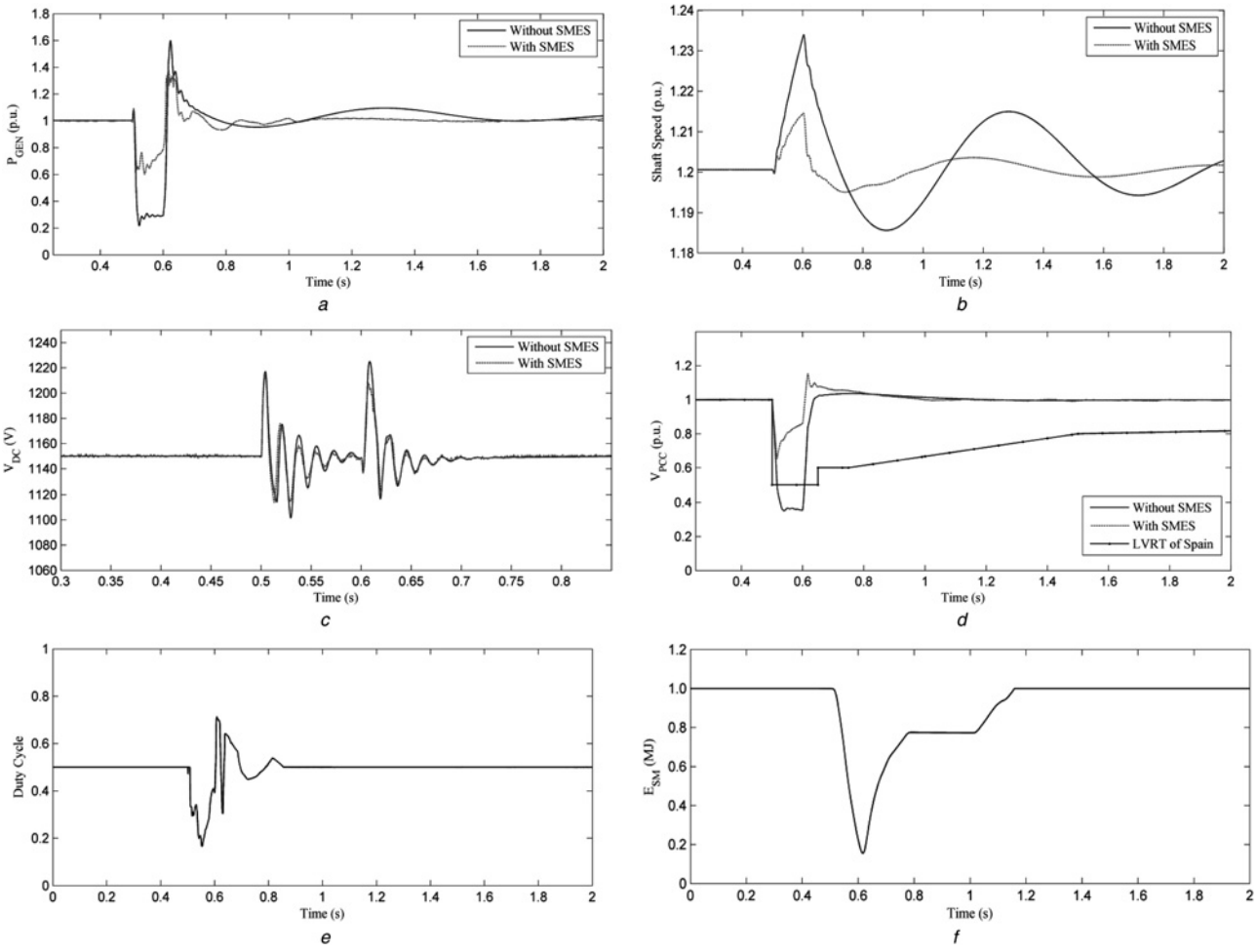

Fig. 12 *Response of the DFIG during a three-phase short-circuit fault at point A*

a Generated power of DFIG
b Rotor shaft speed
c Voltage across DFIG DC link
d Voltage profile at PCC
e Duty cycle response of the SMES unit
f Stored energy response of the SMES unit

of D below 0.5 and the energy stored in the coil is discharged into the grid to provide active power support. When the load returns to its steady-state level, the coil is partially charged but not to its full capacity. When the load is decreased at $t = 4$ s, the value of D is increased because of the controller action to a level above 0.5 and the surplus power in the system will be used to fully charge the SMES coil.

4.2 Large disturbance

To examine the ability of the SMES unit to improve DFIG dynamic performance during a large disturbance, a six-cycle three-phase short-circuit fault is applied at $t = 0.5$ s and is assumed to last for six cycles. Two fault locations are considered; case A where the short-circuit fault is assumed to take place at the grid terminals (point A in Fig. 3) and case B where the fault is located in the middle of the transmission line (point B in Fig. 3).

Case A: Fig. 12*a* shows that the active power generated by the DFIG is reduced by 75% at the instant of fault occurrence and it experiences a maximum overshooting of 60% at the instant of fault clearance. As a result of the generated power reduction, the shaft speed accelerates during the fault and experiences some oscillations after fault clearance as shown in Fig. 12*b* The large amount of power loss will definitely influence the supply for local loads and the power transfer to the grid. If the DFIG is the main power supply to the local load, the economic loss will be significant. The voltage across the DFIG DC-link capacitor (shown in Fig. 12*c*) will experience significant oscillations and overshooting level through fault duration; however, its maximum overshooting remains within the safety margin of 1.2 pu as specified in [38]. The voltage at the point of common coupling (PCC) is reduced to a level of 0.4 pu during the fault. When compared with the Spain FRT requirement, the voltage profile at the PCC violates the permissible lower limit as shown in Fig. 12*c*, which calls for the disconnection of WECS from the grid. When the short circuit is cleared, the DFIG converters act to provide reactive power support to the grid to recover the voltage to its rated value [39]. By connecting the SMES unit to the DFIG bus, the proposed controller acts to change the duty cycle level and hence the energy transfer direction according to the system requirements. As shown in Fig. 12*e*, the duty cycle is reduced below 0.5 during the fault and the entire SMES stored energy will be discharged to support the system during the fault as shown in Fig. 12*f*. As a result, the DFIG generated power will be reduced by

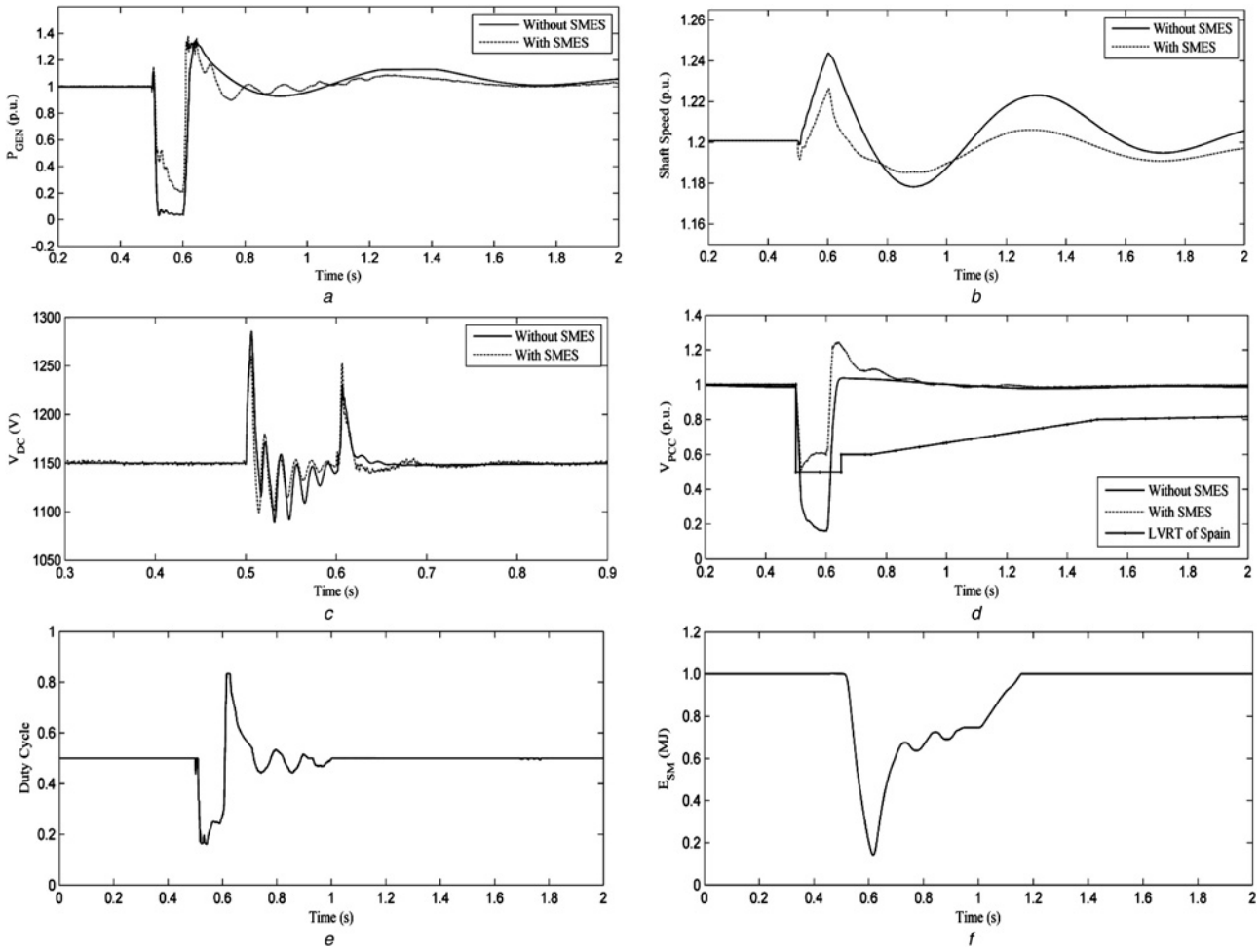

Fig. 13 *Response of the DFIG during a three-phase short-circuit fault at point B*

a Generated power of DFIG
b Rotor shaft speed
c Voltage across DFIG DC link
d Voltage profile at PCC
e Duty cycle response of the SMES unit
f Stored energy response of the SMES unit

doi: 10.1049/iet-pel.2012.0135

only 30% and its maximum overshooting and settling time are substantially reduced as shown in Fig. 12*a*. As a result of this improvement, the acceleration and settling time of the rotor shaft speed will be significantly reduced as can be seen in Fig. 12*b*. There is a slight improvement in the DFIG DC-link voltage (Fig. 12*c*) in terms of the over-shooting levels but as mentioned above, these levels are within the safety margins specified in [38]. Connecting the SMES unit to the system will bring the voltage at the PCC to the safety margin of Spain grid codes as shown in Fig. 12*d*. In this case, the WECS connection to the grid can be maintained to support the grid during the fault duration.

Case B: When a three-phase short-circuit fault occurs at the middle of the transmission line, DFIG generated power drops significantly as shown in Fig. 13*a*. The impact of this fault on the shaft speed and DC-link capacitor voltage is worse when compared with the previous case as shown in Figs. 13*b* and *c*, respectively. Voltage level at the PCC reaches 0.1 pu and it violates the low-voltage ride through level of Spain grid code as shown in Fig. 13*d*. With the SMES unit connected to the PCC bus; the generated power drop can be improved compared with the system without SMES unit as shown in Fig. 13*a*. Also, shaft speed and DC-link voltage as shown in Figs. 13*b* and *c* are improved with the connection of the SMES unit. With the connection of the SMES unit, the connection of the wind turbine to the grid during such fault can be maintained as shown in Fig. 13*d*, where the voltage drop at the PCC is brought to a safety margin of Spain's FRT. The trend of duty cycle and energy stored within the superconductor coil is similar to case A; however, they are slightly larger than those in case A as shown in Figs. 13*e* and *f*.

5 Conclusion

This paper introduces a new application along with a new controller for the SMES unit to improve the dynamic performance and to maintain the connection of WECS to the grid during small and large disturbances. Based on detailed simulation results and analyses it can be concluded that the overall performance of WECS during small and large disturbances can be significantly improved using the proposed SMES controller. The proposed fuzzy-based SMES controller along with hysteresis current regulator is effective, simple and easy to implement. The SMES unit, however, is still a costly device because of the use of a low-temperature superconducting coil. However, the rapid development of a high-temperature superconductor will make the SMES unit one of the most popular FACTS devices in power system applications in the near future.

6 Acknowledgments

The first author would like to thank the Higher Education Ministry of Indonesia (DIKTI) and the State Polytechnic of Ujung Pandang in collaboration with Curtin University for supporting the research.

7 References

1 http://www.wwindea.org, accessed June 2012
2 Global Wind Report: 'Annual market update 2010' (Global Wind Energy Council, 2011)
3 Carrasco, J.M., Franquelo, L.G., Bialasiewicz, J.T., *et al.*: 'Power-electronic systems for the grid integration of renewable energy sources: a survey', *IEEE Trans. Ind. Electron.*, 2006, **53**, pp. 1002–1016
4 Polinder, H., Bang, D.-J., Li, H., Cheng, Z.: 'Concept report on generator topologies, mechanical and electromagnetic optimization'. Project UpWind, 2007
5 Tsili, M., Papathanassiou, S.: 'A review of grid code technical requirements for wind farms', *IET Renew. Power. Gener.*, 2009, **3**, pp. 308–332
6 Seman, S., Niiranen, J., Arkkio, A.: 'Ride-through analysis of doubly fed induction wind-power generator under unsymmetrical network disturbance', *IEEE Trans. Power Syst.*, 2006, **21**, pp. 1782–1789
7 Xiangwu, Y., Venkataramanan, G., Flannery, P.S., Yang, W., Qing, D., Bo, Z.: 'Voltage-sag tolerance of DFIG wind turbine with a series grid side passive-impedance network', *IEEE Trans. Energy Convers.*, 2010, **25**, pp. 1048–1056
8 Hu, S., Lin, X., Kang, Y., Zou, X.: 'An improved low-voltage ride-through control strategy of doubly fed induction generator during grid faults', *IEEE Trans. Power Electron.*, 2011, **26**, pp. 3653–3665
9 Lopez, J., Gubia, E., Olea, E., Ruiz, J., Marroyo, L.: 'Ride through of wind turbines with doubly fed induction generator under symmetrical voltage dips', *IEEE Trans. Ind. Electron.*, 2009, **56**, pp. 4246–4254
10 Slootweg, J.G., de Haan, S.W.H., Polinder, H., Kling, W.L.: 'General model for representing variable speed wind turbines in power system dynamics simulations', *IEEE Trans. Power. Syst.*, 2003, **18**, pp. 144–151
11 Hee-Yeol, J., Kim, A.R., Jae-Ho, K., *et al.*: 'A study on the operating characteristics of SMES for the dispersed power generation system', *IEEE Trans. Appl. Supercond.*, 2009, **19**, pp. 2028–2031
12 Chen, S.S., Wang, L., Lee, W.J., Chen, Z.: 'Power flow control and damping enhancement of a large wind farm using a superconducting magnetic energy storage unit', *IET Renew. Power Gener.*, 2009, **3**, pp. 23–38
13 Ali, M.H., Minwon, P., In-Keun, Y., Murata, T., Tamura, J.: 'Improvement of wind-generator stability by fuzzy-logic-controlled SMES', *IEEE Trans. Ind. Appl.*, 2009, **45**, pp. 1045–1051
14 Zhou, F., Joos, G., Abbey, C., Jiao, L., Ooi, B.T.: 'Use of large capacity SMES to improve the power quality and stability of wind farms'. Power Engineering Society General Meeting, 2004, vol. 2, pp. 2025–2030
15 Sheikh, M.R.I., Muyeen, S.M., Takahashi, R., Murata, T., Tamura, J.: 'Minimization of fluctuations of output power and terminal voltage of wind generator by using STATCOM/SMES'. Power Tech, Bucharest, 2009, pp. 1–6
16 Asao, T., Takahashi, R., Murata, T., *et al.*: 'Smoothing control of wind power generator output by superconducting magnetic energy storage system'. Int. Conf. on Electrical Machines and Systems, 2007, pp. 302–307
17 Hee-yeol, J., Dae-Jin, P., Hyo-Ryong, S., Minwon, P., In-Keun, Y.: 'Power quality enhancement of grid-connected wind power generation system by SMES'. Power Systems Conf. and Exposition, 2009, pp. 1–6
18 Li, W., Shiang-Shong, C., Wei-Jen, L., Zhe, C.: 'Design of a damping controller for a SMES unit to suppress tie-line active-power fluctuations of a large-scale wind farm'. Power Systems Conf. and Exposition, 2009, pp. 1–7
19 Jing, S., Yuejin, T., Yajun, X., Li, R., Jingdong, L.: 'SMES based excitation system for doubly-fed induction generator in wind power application', *IEEE Trans. Appl. Supercond.*, 2011, **21**, pp. 1105–1108
20 Nam, T., Shim, J.W., Hur, K.: 'The beneficial role of SMES coil in dc lines as an energy buffer for integrating large scale wind power', *IEEE Trans. Appl. Supercond.*, 2012, **22**, p. 5701404–5701404
21 Slemon, G.R.: 'Modelling of induction machines for electric drives', *IEEE Trans. Ind. Appl.*, 1989, **25**, pp. 1126–1131
22 Mohseni, M., Islam, S.M., Masoum, M.A.: 'Enhanced hysteresis-based current regulators in vector control of DFIG wind turbines', *IEEE Trans. Power Electron.*, 2011, **26**, pp. 223–234
23 Mohseni, M., Islam, S.M., Masoum, M.A.: 'Impacts of symmetrical and asymmetrical voltage sags on DFIG-based wind turbines considering phase-angle jump, voltage recovery, and sag parameters', *IEEE Trans. Power Electron.*, 2011, **26**, pp. 1587–1598
24 Mohseni, M., Masoum, M.A., Islam, S.M.: 'Emergency control of DFIG-based wind turbines to meet new European grid code requirements' (Innovative Smart Grid Technologies, 2011), pp. 1–6
25 Blaabjerg, F., Chen, Z.: 'Power electronics for modern wind turbines' (Morgan & Claypool Publishers, 2006)
26 Li, H., Chen, Z., Polinder, H.: 'Research report on numerical evaluation of various variable speed wind generator systems' (Institute of Energy Technology, 2006)
27 Freris, L., Infield, D.: 'Renewable energy in power system' (John Wiley & Sons, 2008), pp. 143–144
28 Ribeiro, P.F., Johnson, B.K., Crow, M.L., Arsoy, A., Liu, Y.: 'Energy storage systems for advanced spower applications', *Proc. IEEE*, 2001, **89**, pp. 1744–1756

29 Smith, S.C., Sen, P.K., Kroposki, B.: 'Advancement of energy storage devices and applications in electrical power system'. Power and Energy Society General Meeting, 2008, pp. 1–8
30 Abu-Siada, A., Islam, S.: 'Application of SMES unit in improving the performance of an AC/DC power system', *IEEE Trans. Sustain. Energy*, 2011, **2**, pp. 109–121
31 Hassan, I.D., Bucci, R.M., Swe, K.T.: '400 MW SMES power conditioning system development and simulation', *IEEE Trans. Power Electron.*, 1993, **8**, pp. 237–249
32 Ackerman, T.: 'Wind power in power system' (John Wiley & Sons Ltd., 2005)
33 Kim, A.R., Hyo-Ryong, S., Gyeong-Hun, K., *et al.*: 'Operating characteristic analysis of HTS SMES for frequency stabilization of dispersed power generation system', *IEEE Trans. Appl. Supercond.*, 2010, **20**, pp. 1334–1338
34 Molina, M.G., Mercado, P.E.: 'Power flow stabilization and control of microgrid with wind generation by superconducting magnetic energy storage', *IEEE Trans. Power Electron.*, 2011, **26**, pp. 910–922
35 Bong-Hwan, K., Tae-Woo, K., Jang-Hyoun, Y.: 'A novel SVM-based hysteresis current controller', *IEEE Trans. Power Electron.*, 1998, **13**, pp. 297–307
36 Carlsson, A.: 'The back to back converter' (Department of Industrial Electrical Engineering and Automation Lund Institute of Technology, Lund, 1998)
37 Li, H., Gupta, M.M.: 'Fuzzy logic and intelligent system' (Kluwer Academic Publisher, 1995)
38 Akhmatov, V.: 'Analysis of dynamic behaviour of electric power system with large amount of wind power'. PhD thesis, Technical University of Denmark, 2003
39 Boussean, P., Gautier, E., Garzulino, I., Juston, P., Belhomme, R.: 'Grid impact of different technologies of wind turbine generator systems' (EDF Electricite de France, Clamart Cedex, 2003)

8 Appendix

The parameters of DFIG are presented in Table 2.

Parameters of DFIG

Rated power	9 MW (6× at 1.5 MW)
Stator voltage	575 V
Frequency	60 Hz
R_s	0.023 p.u.
R_r	0.016 p.u.
V_{DC}	1150 V

doi: 10.1049/iet-pel.2012.0135